

Diffusion coefficients in leaflets of bilayer membranes

Kazuhiko Seki

NRI, National Institute of Advanced Industrial Science and Technology (AIST)

AIST Central 5, Higashi 1-1-1, Tsukuba, Ibaraki 305-8565, Japan,

Saurabh Mogre

Indian Institute of Technology Bombay,

Powai, Mumbai, Maharashtra 400 076, India

Shigeyuki Komura

Department of Chemistry, Graduate School of Science and Engineering,

Tokyo Metropolitan University, Tokyo 192-0397, Japan

Abstract

We study diffusion coefficients of liquid domains by explicitly taking into account the two-layered structure called leaflets of the bilayer membrane. In general, the velocity fields associated with each leaflet are different and the layers sliding past each other cause frictional coupling. We obtain analytical results of diffusion coefficients for a circular liquid domain in a leaflet, and quantitatively study their dependence on the inter-leaflet friction. We also show that the diffusion coefficients diverge in the absence of coupling between the bilayer and solvents, even when the inter-leaflet friction is taken into account. In order to corroborate our theory, the effect of the inter-leaflet friction on the correlated diffusion is examined.

PACS numbers:

I. INTRODUCTION

Diffusion of inclusions in membranes occurs in 2-dimensional (2D) media embedded in solvents, and is different from that in a homogeneous 3-dimensional (3D) fluid. In the pioneering work by Saffmann and Delbrück [1, 2], the membrane was regarded as a thin plane sheet bounded on both sides by solvents. Solvents are dragged by the flow in the membrane through the coupling to the solvent flow at the solvent/membrane interfaces. The transfer of momentum between the membrane and solvents necessitates the introduction of a length called the Saffmann-Delbrück (SD) hydrodynamic screening length [1–3]. The SD expression of the diffusion coefficient has been elaborated to apply to the larger size of objects [4]. Although some experiments were not explained by the SD theory [5], the SD theory and its extended expressions have been supported by certain experiments [6–8].

When the membrane is supported on a solid substrate, a very thin layer of solvent exists between the membrane and the solid support [9]. For supported membranes, the assumption of infinite thickness of solvents in SD theory is irrelevant; the diffusion coefficient decreases when the thickness of solvent layer is decreased [9, 10]. The length scale of momentum transfer is characterized by a new length scale, called Evans-Sackmann (ES) hydrodynamic screening length in the limit of thin layer of solvent. When the size of the diffusing object exceeds the ES hydrodynamic screening length, the diffusion coefficient is predicted to show the inverse square size-dependence [9]. The inverse square size-dependence has been observed in supported lipid bilayers [11].

In the earlier works, diffusion of solid molecules in homogeneous membranes has been studied. Recently, microheterogeneity of the membrane has attracted great interest [12–15]. The micro-domains in multicomponent membranes have been expected to be involved in signal transduction and control intracellular transport [12–15]. By phase separation of ternary mixtures of cholesterol, saturated and unsaturated lipids, regions rich in saturated lipids and cholesterol coexist with those rich in unsaturated lipids. The smaller regions form circular viscous domains and diffuse laterally. The diffusion coefficients of liquid domains have been obtained using hydrodynamic calculations by ignoring a shear flow across the membrane [16–20]. However, it is possible to form membranes with bilayer consisting of two leaflets having different compositions [14, 15]. The liquid domains in each leaflet do not necessarily lie on top of one another; the liquid domains can be formed in one of the

leaflets without overlapping to those in the other leaflet. In general, the velocity fields associated with each leaflet are different and the layers sliding past each other cause frictional coupling [21–25].

When relative motion of the leaflets does not play a significant role, the bilayer can be considered as a single fluid medium. However, the inter-leaflet friction would induce different transport in two leaflets of the bilayer for supported membranes, because each leaflet faces different environment [24]. Furthermore, when the solvent thickness is small, typical for supported membranes, the relative velocity difference between the wall and the membrane induces a shear flow in the solvent through the stick boundary condition. The resultant drag force from the solvent can be sufficiently large to decouple the two leaflets.

The diffusion of solid particles in a leaflet under the inter-leaflet friction was previously studied numerically [24]. The complex interplay between the inter-leaflet friction and the drag from solvents was shown. In this paper, we derive analytical results of diffusion coefficients for circular liquid domains. Although we use the same mobility tensor derived by Brown *et al.* [24], we present the analytical expressions showing the effect of the inter-leaflet friction on the diffusion coefficients for the general thickness of solvent. By examining the asymmetry in diffusion coefficients associated with the upper and lower leaflet for supported membranes, we find that the value of inter-leaflet friction can be estimated. In addition, we show that the momentum is dissipated by the inter-leaflet friction, but this dissipation mechanism is not sufficient to overcome logarithmic long-range correlations in the flow fields leading to a divergence of the diffusion coefficient. In order to corroborate our theory, the correlated diffusion is studied under the influence of the inter-leaflet friction.

In experiments, the frictional interaction between the leaflets has been studied in detail by applying the interlayer shear stress induced by a large local deformation [26–29]. Zhang and Granick concluded that the difference in diffusion coefficient of lipids between two leaflets is small for supported bilayers [30]. Detailed investigation on diffusion of lipids in leaflets on supported membranes suggests that the diffusion coefficient of lipids in the lower leaflet is reduced from that of the upper leaflet depending on the type of substrate [31–33].

Simulations have been also performed to estimate the value of inter-leaflet friction [34–36]. From coarse-grained molecular simulations, the lateral diffusion of lipids in the lower leaflet to the solid substrate was shown to be slower than that of the upper leaflet by one order of magnitude [36]. We discuss the results on the asymmetry in diffusion coefficients

for the supported membranes using the values of the inter-leaflet friction thus estimated.

In Sec. II, the diffusion coefficient of a circular domain in a bilayer membrane is obtained by taking into account the inter-leaflet friction for arbitrary thickness and viscosity of solvents. In Sec. III, we study the effect of the inter-leaflet friction on the SD length and ES length. Symmetric environments are considered for simplicity. Diffusion in a supported bilayer is considered in Sec. IV. In Sec. V, we study correlated dynamics of two point particles. In Sec. VI, we show that the finite diffusion coefficient cannot result from the inter-leaflet friction alone without solvents. The final section is devoted for summary and discussion.

II. THE DIFFUSION COEFFICIENT OF A CIRCULAR DOMAIN IN A LEAFLET

A. Hydrodynamic model

We explicitly take into account the two-layered structure of the membrane as shown in Fig. 1. The structure is sometimes referred to as the leaflets and its hydrodynamics has been studied previously [21, 24]. These leaflets are denoted by the indices “+” and “−” for the upper and lower monolayer, respectively. The monolayers of the membrane, called leaflets, are coupled through the drag force between the upper and lower leaflets.

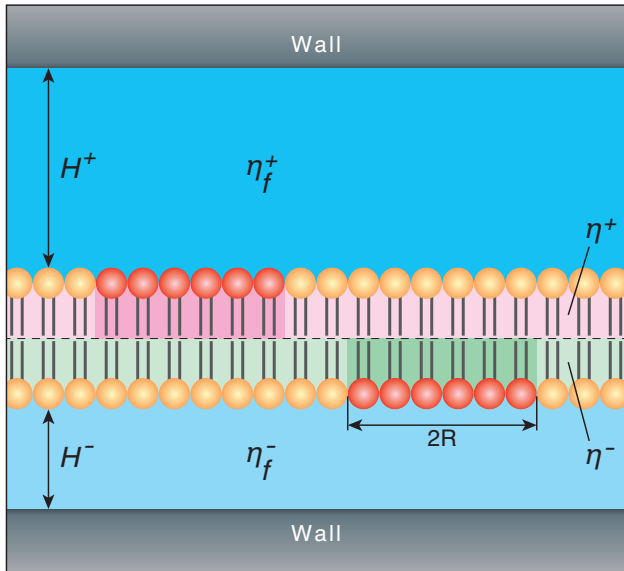


FIG. 1: (Color online) The geometry of the bilayer in a general environment. Liquid domains of size $2R$ diffuse in leaflets.

We consider a circular liquid domain of radius R which is immersed in either leaflet. For simplicity, we assume that the viscosity of the liquid inside the domain is the same as that of the leaflet in which the domain is located. We also assume that the domain maintains a circular shape by the line tension and does not undergo deformation as it moves. The system is illustrated in Fig. 1. We will derive the general expression for the diffusion coefficient in either case.

The 2D viscosity of the leaflets are denoted by η^\pm , depending on the upper or lower leaflet. The bilayer membrane is sustained in a solvent at distance H^+ and H^- below and above the walls, respectively. The viscosity of the solvent above and below the membrane is represented by η_f^+ and η_f^- , respectively.

The in-plane flow in each leaflet can be described using Stokes equations with additional terms associated with the coupling between the leaflet and the solvent through the interface and the friction between leaflets [21–24],

$$\eta^\pm \nabla^2 \mathbf{v}^\pm - \nabla p^\pm + K^\pm * \mathbf{v}^\pm \mp \Lambda(\mathbf{v}^+ - \mathbf{v}^-) + \mathbf{f}^\pm = 0, \quad (1)$$

with the incompressibility condition,

$$\nabla \cdot \mathbf{v}^\pm = 0, \quad (2)$$

where p^\pm and \mathbf{v}^\pm indicate the hydrodynamic pressure and fluid velocities of the leaflets, respectively. In the above, the position vector \mathbf{r} is abbreviated. The term $\Lambda(\mathbf{v}^+ - \mathbf{v}^-)$ accounts for the frictional coupling between the two leaflets. The convolution term $K^\pm * \mathbf{v}^\pm = \int d^2r' K^\pm(\mathbf{r} - \mathbf{r}') \mathbf{v}^\pm(\mathbf{r}')$ represents the drag from the solvent. Using Fourier transform $\hat{K}(\mathbf{k}) = \int d^2r \exp(-i\mathbf{k} \cdot \mathbf{r}) K(\mathbf{r})$, the convolution can be expressed as a product. The drag force from the solvent depends on the geometry of the system. For the system under consideration, we have $\hat{K}^\pm = -\eta_f^\pm k \coth(kH^\pm)$ for arbitrary solvent thickness [37–40]. The external in-plane force is denoted by \mathbf{f}^\pm .

B. Diffusion coefficient

We consider the case when the circular domain moves with a velocity \mathbf{U} in leaflet α . The origin of the coordinates is taken to be the center of the domain and the x -coordinate is chosen in the direction of \mathbf{U} . The external in-plane force applied at the periphery of the

circular domain in Eq. (1) is given by $\mathbf{f}^\pm = f^{(\ell n)} \cos \theta \mathbf{n} \delta(r - R)/(2\pi R)$ [16], where \mathbf{n} is the outward normal unit vector on the circumference of the domain, θ is the angle between \mathbf{U} and \mathbf{r} , and $\cos \theta$ term reflects the symmetry of the system. $f^{(\ell n)}$ is a constant which should give the external force after the integration over the circular domain boundary.

We can derive the diffusion coefficient of the circular domain in either leaflet using a similar method as in our previous publication [18]. By introducing a component of a mobility tensor in Fourier space given in the Appendix A [24], the diffusion coefficient of the liquid domain is obtained as,

$$D_{dom}^\alpha = k_B T \int_0^\infty dk \frac{[J_1(kR)]^2}{\pi k R^2} \left[\frac{\eta^{(-\alpha)} k^2 + \eta_f^{(-\alpha)} k \coth(kH^{(-\alpha)}) + \Lambda}{\prod_\alpha (\eta^{(\alpha)} k^2 + \eta_f^{(\alpha)} k \coth(kH^{(\alpha)}) + \Lambda) - \Lambda^2} \right], \quad (3)$$

where α denotes the leaflet, $-\alpha$ denotes the leaflet opposite to α and $J_1(z)$ denotes the Bessel functions of the first kind of order 1 [41].

The expression for the diffusion coefficient contains various physical quantities with varying magnitudes and different units. In order to systematically compare various cases and to have a concise understanding of the results, we make the variables dimensionless mainly using the SD hydrodynamic screening length given by $1/\nu^\pm \equiv \eta^\pm/\eta_f^\pm$ [1–3]. The following dimensionless variables are defined:

$$\rho^\pm = \nu^\pm R, \quad h^\pm = \nu^\pm H^\pm, \quad \lambda^\pm = \frac{\Lambda}{\eta^\pm} \frac{1}{(\nu^\pm)^2}, \quad \mu = \frac{\eta^-}{\eta^+}. \quad (4)$$

Here, ρ^\pm and h^\pm represent the dimensionless radius of the liquid domain and the dimensionless solvent thickness, respectively. The ES hydrodynamic screening length is given by the smaller of $\sqrt{h^\pm}/\nu$. A new length, $\sqrt{\eta^-/\Lambda}$, is associated with the inter-leaflet friction. This quantity can be called the inter-leaflet sliding length, and contributes to the hydrodynamic screening factor in addition to the contribution from the solvent. The variable μ is the ratio between the 3D-viscosities of the leaflets. In the later sections, the index of the dimensionless variables is dropped when it is redundant, *e.g.* $h = h^\pm$ whenever it is clear from the context or the variables do not differ between the indices.

III. DIFFUSION FOR A LIQUID DOMAIN IN A SYMMETRIC ENVIRONMENT

For simplicity we consider the symmetric system as illustrated in Fig. 2. We assume a solvent layer of equal thickness on both sides of the membrane, *i.e.* $H^+ = H^- = H$. The

viscosity of the solvents and two leaflets are also taken to be equal, i.e. $\eta_f^+ = \eta_f^- = \eta_f$ and $\eta^+ = \eta^- = \eta$.

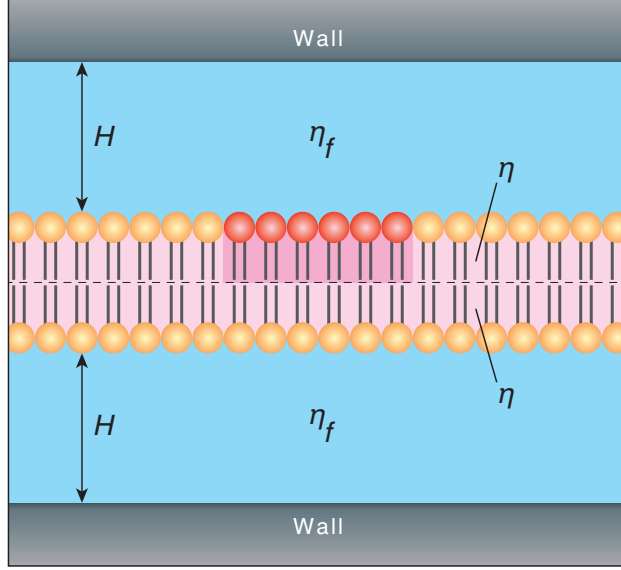


FIG. 2: (Color online) The geometry of the bilayer in a symmetric environment. Liquid domains of size $2R$ shown by red diffuse in leaflets.

For this case, the diffusion coefficient is simplified to,

$$D_{sym} = \frac{1}{2} [D_0 + D_1(\lambda)], \quad (5)$$

where

$$D_1(\lambda) = \frac{k_B T}{\pi \eta \rho^2} \int_0^\infty d\kappa \frac{[J_1(\kappa \rho)]^2}{\kappa} \left[\frac{1}{\kappa^2 + \kappa \coth(\kappa h) + 2\lambda} \right]. \quad (6)$$

In the above, D_0 represents $D_1(\lambda = 0)$, which is the case in the absence of the inter-leaflet friction. [18]

We can see from Eq. (5) and Fig. 3 that the diffusion coefficient decreases from D_0 to $D_0/2$ as the inter-leaflet friction is changed from 0 to ∞ . The qualitatively similar behavior is obtained by Camley and Brown for a solid circular object in a freely suspended membrane when the symmetric leaflets are faced to the same solvent medium [24]. We also note in Fig. 3 that the diffusion coefficient as a function of λ behaves very differently when $\rho \ll 1$. The reason is separately discussed in Appendix C.

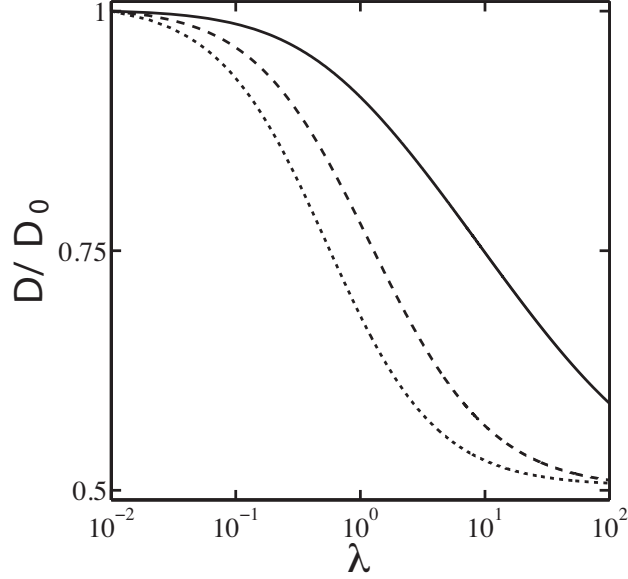


FIG. 3: Normalized diffusion coefficient D/D_0 as a function of λ for $h = 1$ is shown by using Eq. (5). Here, $D_0 = D(\lambda = 0)$. The values of $\pi\eta D_0/(k_B T)$ are $0.5882(\rho = 0.1)$, $0.1404(\rho = 1)$, and $0.0044(\rho = 10)$. The solid, dashed and dotted lines represent $\rho = 0.1, 1, 10$, respectively.

A. Infinite solvent medium

In the limit of $H \rightarrow \infty$, we have $\coth(\kappa h) \approx 1$ in Eq. (6). The expression for the diffusion coefficient becomes

$$D_{sym} = \frac{k_B T}{2\pi\eta\rho^2} \int_0^\infty d\kappa \frac{[J_1(\kappa\rho)]^2}{\kappa} \left[\frac{1}{\kappa^2 + \kappa} + \frac{1}{\kappa^2 + \kappa + 2\lambda} \right]. \quad (7)$$

The above integral can be calculated by using Mathematica and is expressed in terms of Meijer-G functions [42, 43],

$$D_{sym} = \frac{k_B T}{4\pi\eta\rho^2} \left[\frac{1}{\sqrt{1-8\lambda}} \left\{ \frac{1}{\pi^{3/2}c_1} G_{2,4}^{3,2} \left((c_1\rho)^2 \left| \begin{matrix} \frac{1}{2}, \frac{1}{2} \\ 0, \frac{1}{2}, 1, -1 \end{matrix} \right. \right) - \frac{1}{\pi^{3/2}c_2} G_{2,4}^{3,2} \left((c_2\rho)^2 \left| \begin{matrix} \frac{1}{2}, \frac{1}{2} \\ 0, \frac{1}{2}, 1, -1 \end{matrix} \right. \right) \right\} + \frac{1}{2\lambda} - 1 - \frac{1}{\pi^{3/2}} G_{2,4}^{3,2} \left(\rho^2 \left| \begin{matrix} \frac{1}{2}, \frac{3}{2} \\ 0, 1, \frac{3}{2}, -1 \end{matrix} \right. \right) \right], \quad (8)$$

where c_1 and c_2 are the roots of the quadratic equation, $\kappa^2 + \kappa + 2\lambda = 0$. The limits for the domain size can now be taken to this expression.

By taking the limit of small domain size, i.e., $\rho \ll 1$, $c_1\rho \ll 1$, and $c_2\rho \ll 1$, in Eq. (8), the diffusion coefficient is shown to depend logarithmically on the domain size,

$$D_{sym} \approx \frac{k_B T}{4\pi\eta} \left[\ln \left(\frac{2\eta}{\eta_f R} \right) - \gamma + \frac{1}{4} + \frac{1}{2(c_1 - c_2)} (c_2 \ln c_2 - c_1 \ln c_1) \right], \quad (9)$$

where $\gamma = 0.5772\dots$ is Euler's constant [41].

By taking the limit of large domains, i.e. $c_1\rho \gg 1$, $\rho \gg 1$ and $c_2\rho \gg 1$, in Eq. (8), we obtain,

$$D_{sym} \approx \frac{2k_B T}{3\pi^2\eta_f R} + \frac{k_B T}{8\pi R^2} \left(\frac{1}{\Lambda} - \frac{2\eta}{\eta_f^2} \right). \quad (10)$$

In the asymptotic limit of large domain size, the diffusion coefficient is independent of the membrane viscosity η . The asymptotic domain size-dependence is given by the first term, $1/R$, which is independent of the inter-leaflet friction. The second term showing $1/R^2$ -dependence is associated with the inter-leaflet friction.

Equation (10) implies that the diffusion coefficient depends on λ if it is smaller than $\lambda_{sym}^* = 3\pi/(16\rho)$. By plotting the diffusion coefficient as a function of λ as shown in Fig. 3, we confirm that the inflection point where D_{sym} depends most strongly on λ , can be estimated by using λ_{sym}^* when $\rho \geq 0.1$.

B. Thin solvent medium

In the limit of, $H \rightarrow 0$, we have $\coth(\kappa h) \approx 1/\kappa h$ in Eq. (6). By taking this limit, the expression for the diffusion coefficient becomes

$$D_{sym} = \frac{k_B T}{2\pi\eta\rho^2} \int_0^\infty d\kappa \frac{[J_1(\kappa\rho)]^2}{\kappa} \left[\frac{1}{\kappa^2 + 1/h + 2\lambda} + \frac{1}{\kappa^2 + 1/h} \right]. \quad (11)$$

We can analytically integrate Eq. (11) and the result is given by,

$$D_{sym} = \frac{k_B T}{2\pi R^2} \left\{ \frac{H}{\eta_f} \left[\frac{1}{2} - I_1 \left(R \sqrt{\frac{\eta_f}{\eta H}} \right) K_1 \left(R \sqrt{\frac{\eta_f}{\eta H}} \right) \right] + \frac{1}{(\eta_f/H) + 2\Lambda} \left[\frac{1}{2} - I_1 \left(R \sqrt{\frac{(\eta_f/H) + 2\Lambda}{\eta}} \right) K_1 \left(R \sqrt{\frac{(\eta_f/H) + 2\Lambda}{\eta}} \right) \right] \right\}. \quad (12)$$

By taking the limit of $\rho \ll 1$, $\rho/\sqrt{h} \ll 1$ and $\rho/\sqrt{(1/h) + 2\lambda} \ll 1$ in Eq. (12), we obtain,

$$D_{sym} \approx \frac{k_B T}{4\pi\eta} \left[\ln \left(\frac{2}{R} \sqrt{\frac{\eta_f H}{\eta}} \frac{1}{[1 + (2\Lambda H/\eta_f)]^{1/4}} \right) - \gamma + \frac{1}{4} \right]. \quad (13)$$

As in the case of an infinite solvent medium, Eq. (9), the diffusion coefficient is shown to depend logarithmically on the domain size.

By taking the limit of $\rho \gg 1$, $\rho/\sqrt{h} \gg 1$ and $\rho/\sqrt{(1/h) + 2\lambda} \gg 1$, Eq. (12) reduces to,

$$D_{sym} \approx \frac{k_B T H}{2\pi\eta_f R^2} \left[\frac{1 + \Lambda H/\eta_f}{1 + 2\Lambda H/\eta_f} \right]. \quad (14)$$

As in the case of an infinite solvent medium, the diffusion coefficient is independent of the membrane viscosity. The diffusion coefficient shows $1/R^2$ -dependence in this limit, which is stronger than that in Eq. (10). The size dependence of the diffusion coefficient is qualitatively the same as that obtained by regarding the membrane as a sheet of 2D fluid without any leaflet structure, though there are quantitative differences given by $\Lambda H/\eta_f$ -dependence.

C. Arbitrary thickness of solvent medium

The integrand in Eq. (6) can be expressed by a sum using the partial fraction expansion as shown in Appendix B. The result after the integration is given as

$$D_{sym} = \frac{k_B T}{2\pi\eta\rho^2} \sum_{s=1}^{\infty} \left\{ W'_s \left[\frac{1}{2} - I_1(\omega'_s \rho) K_1(\omega'_s \rho) \right] + W_s \left[\frac{1}{2} - I_1(\omega_s \rho) K_1(\omega_s \rho) \right] \right\}, \quad (15)$$

where the weight factor is given by

$$W_s = \frac{2}{h\omega_s^4 + (1 + h - 4\lambda h)\omega_s^2 + 2\lambda + 4h\lambda^2} \quad (16)$$

and ω_s satisfies the characteristic equation,

$$\omega_s^2 = \omega_s \cot(\omega_s h) + 2\lambda. \quad (17)$$

In the above, $W'_s = 2/[\omega_s'^2(1 + h + \omega_s'^2 h)]$ and $\omega'_s = \cot(\omega'_s h)$ are W_s and ω_s obtained by setting $\lambda = 0$, respectively. Moreover, $I_1(z)$ and $K_1(z)$ are the modified Bessel functions of order 1 [41]. We can show that the rigorous condition for $H \rightarrow 0$ to obtain Eq. (12) is $h = \nu H < \pi$. This is the condition to obtain Eq. (12) from Eq. (15) by retaining the first term in the expansion and ignore the rest.

In the above, $1/(\omega_s \nu)$ represents the hydrodynamic screening length under the inter-leaflet friction. The diffusion coefficient is given by the infinite sum of the expression associated with different hydrodynamic screening lengths. In this sense, hydrodynamic screening is related

to multiple length scales given by $1/(\omega_s \nu)$ with $s = 1, 2, 3, \dots$. The weight approximately satisfies the relation $W_s \sim 1/\omega_s^4$. In the below, we assume that $1/(\omega_s \nu)$ is sorted from small to large values. The difference between the successive screening length, $1/(\omega_s \nu)$ and $1/(\omega_{s+1} \nu)$, is approximately equal to π/h . The weight factor W_s rapidly decreases if $h = \nu H < \pi$. In this case, $1/(\omega_1 \nu)$ can be regarded as the virtual hydrodynamic screening length. The difference due to retaining only the first term in the diffusion coefficient is numerically investigated, and it is at most 10% when $h = 1$. The difference increases by increasing the value of h .

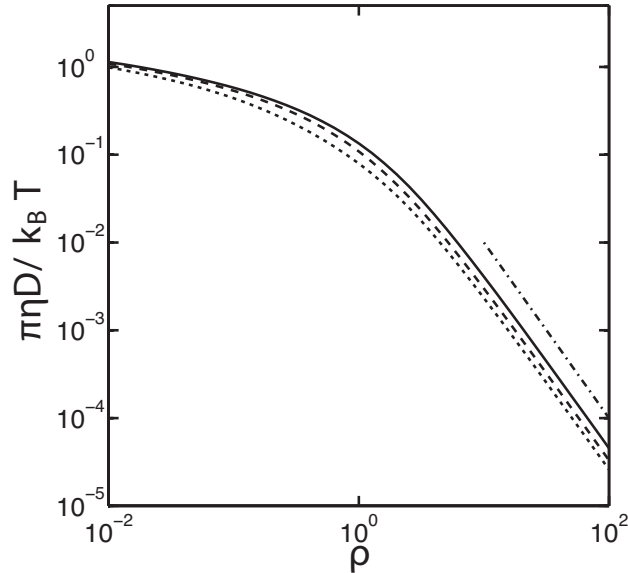


FIG. 4: $\pi\eta D/k_B T$ as a function of ρ for $h = 1$ is shown by using Eq. (5). The solid, dashed and dotted lines represent $\lambda = 0.1, 1, 10$, respectively. The dash-dot line indicates the asymptotic $1/\rho^2$ dependence.

In Fig. 4 we show the diffusion coefficient as a function of the domain size. The diffusion coefficient decreases by increasing λ . When ρ is small, the variation of the diffusion coefficients for the different values of the inter-leaflet friction decreases. This can be understood by noticing that the diffusion coefficient depends logarithmically on the strength of the inter-leaflet friction.

IV. DIFFUSION IN A SUPPORTED BILAYER

In this section, we consider the case where asymmetry in the system is introduced by changing the thickness of the solvent layer above and below the membranes. The values of the viscosities are kept the same as in the symmetric case for simplicity, although a similar calculation is possible with different values as well. Figure 5 illustrates the system being considered.

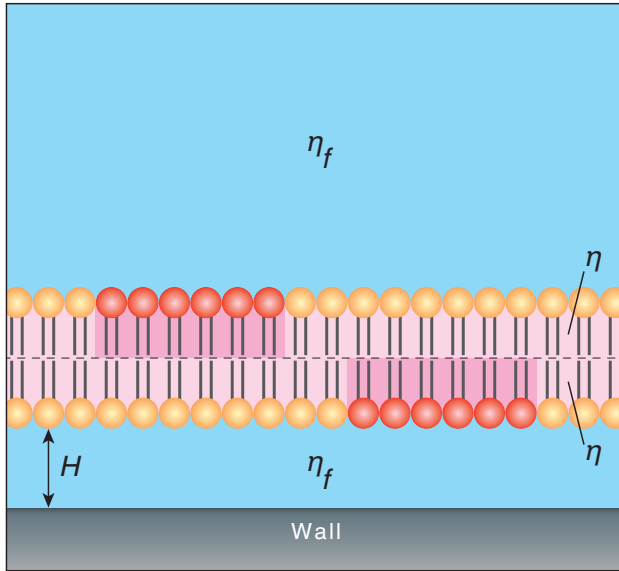


FIG. 5: (Color online) The geometry of the bilayer in an asymmetric environment. Liquid domains of size $2R$ shown by red diffuse in leaflets.

A. Formally exact results

We note that the domain under consideration can be located in either of the two leaflets and diffuses differently in each case. We denote the diffusion coefficient when the domain is in the upper and lower leaflets by D^+ and D^- , respectively.

The situation of supported bilayer can be mathematically expressed as $H^+ \rightarrow \infty$ and $\nu^- H^- \ll 1$. In this limit, we have $\coth(\kappa h^+) \approx 1$ and $\coth(\kappa h^-) \approx 1/\kappa h^-$. By taking above limits and using Eq. (3), the expression for the diffusion coefficient becomes,

$$D_{sup}^\alpha = \frac{k_B T}{\pi \eta \rho^2} \int_0^\infty d\kappa \frac{[J_1(\kappa \rho)]^2}{\kappa} \left[\frac{g^\alpha(\kappa)}{g^+(\kappa)g^-(\kappa) - \lambda^2} \right], \quad (18a)$$

where g^α is given by,

$$g^+(\kappa) = \kappa^2 + \frac{1}{h} + \lambda, \quad (18b)$$

and

$$g^-(\kappa) = \kappa^2 + \kappa + \lambda, \quad (18c)$$

respectively.

As before, by applying a partial fraction expansion to Eq. (18), we obtain [42]

$$D_{sup}^\alpha = \frac{k_B T}{\pi \eta \rho^2} \sum_{i=1}^4 \frac{g^\alpha(\omega_i)}{f'(\omega_i)} \left(\frac{-1}{2\omega_i} \right) \left[1 - \frac{1}{\pi^{3/2}} G_{2 \ 4}^3 \left((\omega_i \rho)^2 \left| \begin{matrix} \frac{1}{2}, \frac{1}{2} \\ 0, \frac{1}{2}, 1, -1 \end{matrix} \right. \right) \right], \quad (19)$$

where ω_i are the roots of the denominator, $f(\kappa) = g^+(\kappa)g^-(\kappa) - \lambda^2 = 0$ and their real parts are negative, while $f'(\kappa)$ is the derivative of the denominator with respect to κ . We note that ω_i are independent of ρ , and use this fact in understanding the size dependence.

As in the previous section, by taking limits of ρ in Eq. (19), we obtain for $\omega_i \rho \ll 1$,

$$D_{sup}^\alpha \approx \frac{k_B T}{4\pi \eta} \sum_{i=1}^4 \frac{\omega_i g^\alpha(\omega_i)}{f'(\omega_i)} \left[\ln \left(\frac{2}{\omega_i \rho} \right) - \gamma + \frac{1}{4} \right], \quad (20)$$

and for $\omega_i \rho \gg 1$

$$D_{sup}^\alpha \approx \frac{k_B T}{2\pi \eta} \sum_{i=1}^4 \frac{g^\alpha(\omega_i)}{f'(\omega_i)} \left(\frac{-1}{\omega_i \rho^2} \right). \quad (21)$$

As in the previous case, the diffusion coefficient depends logarithmically on the domain size for small domains, or the inverse square of the domain size for large domains.

B. Approximate results

Although we have obtained the formal solution, Eq. (19), in terms of the roots of a fourth order polynomial equation, finding the λ or h dependence of the roots is a formidable task. In order to avoid this difficulty, we simplify the model by taking the limit of $\eta_f^+ \rightarrow 0$. When the solvent is water, the solvent viscosity is about two order of magnitude smaller than that of lipids. The limit of $\eta_f^+ \rightarrow 0$ could be justified for a wide range of the values of h , λ and ρ . We thoroughly investigate the mathematical structure of the diffusion constant in the limit of $\eta_f^+ \rightarrow 0$. Then, we compare the analytical solution in the limit of $\eta_f^+ \rightarrow 0$ and that with a finite η_f^+ .

By taking $\eta_f^+ = 0$ in Eq. (3) and assuming that the solvent layer below the membrane is very thin, i.e., $\nu^- H^- \ll 1$, we get,

$$D_{sup}^\alpha = \frac{k_B T}{\pi \eta^- \rho^2} \int_0^\infty d\kappa \frac{[J_1(\kappa \rho)]^2}{\kappa} \left[\frac{g^\alpha(\kappa)}{g^+(\kappa)g^-(\kappa) - \lambda^- \lambda^+} \right], \quad (22a)$$

where we denote

$$g^+(k) = \kappa^2 + 1/h^- + \lambda^-, \quad g^-(k) = \kappa^2 + \lambda^+. \quad (22b)$$

For simplicity, we consider the case when the viscosity of the upper leaflet is the same as that of the lower leaflet.

The integral of Eq. (22a) can be evaluated analytically to give,

$$D_{sup}^\alpha = \frac{k_B T}{\pi R^2} \left[\frac{d^\alpha}{2b} + \frac{H}{\eta_f} \frac{1}{c^+ - c^-} \left\{ \left(1 - \frac{d^\alpha}{c^-}\right) I_1 \left(R \sqrt{\frac{\nu c^-}{H}} \right) K_1 \left(R \sqrt{\frac{\nu c^-}{H}} \right) - \left(1 - \frac{d^\alpha}{c^+}\right) I_1 \left(R \sqrt{\frac{\nu c^+}{H}} \right) K_1 \left(R \sqrt{\frac{\nu c^+}{H}} \right) \right\} \right], \quad (23a)$$

where we have introduced the notations,

$$d^+ = 1 + \frac{\Lambda H}{\eta_f}, \quad d^- = \frac{\Lambda H}{\eta_f}, \quad (23b)$$

and

$$c^\pm = \frac{1}{2} \left[1 + 2 \frac{\Lambda H}{\eta_f} \pm \sqrt{1 + \left(2 \frac{\Lambda H}{\eta_f} \right)^2} \right], \quad (23c)$$

where the double sign corresponds. The first term shows $1/R^2$ size-dependence. It is independent of the membrane viscosity, and is a linear function of the inverse of the inter-leaflet friction constant. It can be seen from Eq. (23) that when $1 \approx 2\Lambda H/\eta_f$ ($1/h \approx 2\lambda$), D changes rapidly by changing the inter-leaflet friction coefficient. The diffusion coefficient as a function of λ for a supported bilayer is shown in Fig. 6. Though the argument is not rigorous, we see from Fig. 6 that the diffusion coefficient indeed changes when λ is close to the above mentioned value. This value is equal to λ_2^* obtained for the domain in a symmetric environment (see Appendix C for detailed discussion on λ_2^*). By decreasing ρ , we note that the inflection point is not characterized by λ_2^* but is close to λ_1^* as in the case of a symmetric environment. (see Appendix C for the detailed discussion on λ_1^*).

For $R\sqrt{\nu c^\alpha/H} \ll 1$, Eq. (23a) can be expanded to yield,

$$D_{sup}^\alpha \approx \frac{k_B T}{4\pi \eta} \left[\ln \left(\frac{2}{R} \sqrt{\frac{\eta_f H}{\eta}} \left(\frac{\eta_f}{\Lambda H} \right)^{1/4} \right) - \gamma + \frac{1}{4} + \frac{\ln(c^\alpha/c^{(-\alpha)})}{4\sqrt{1 + (2\Lambda H/\eta_f)^2}} \right], \quad (24)$$

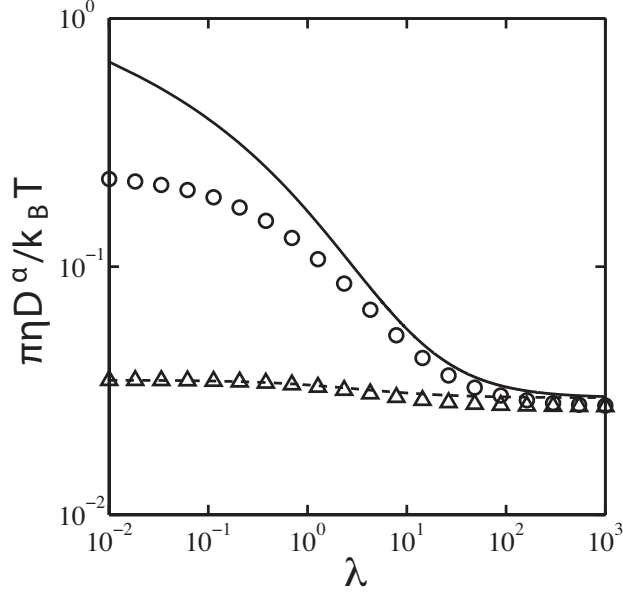


FIG. 6: $\pi\eta D^\alpha/k_B T$ as a function of λ is shown for $h = 0.1$ and $\rho = 1$. The circular and triangular markers denote D^+ and D^- for the supported case, while, the solid and the dashed lines denote D^+ and D^- in the limit of $\eta_f^+ \rightarrow 0$, respectively.

where $(-\alpha)$ represents the leaflet opposite to α as before. The diffusion coefficient shows a logarithmic size-dependence in this limit. The condition, $R\sqrt{\nu c^\alpha/H} \ll 1$, cannot be satisfied in the $\Lambda \rightarrow \infty$ limit because c^α given by Eq. (23) diverges. The order of the limit is important in this respect.

For $R\sqrt{\nu c^\alpha/H} \ll 1$, the diffusion coefficient simplifies into

$$D_{sup}^\alpha \approx \frac{k_B T d^\alpha}{2\pi R^2 \Lambda}. \quad (25)$$

This diffusion coefficient scales with the domain size as $1/R^2$. In this limit, D_{sup}^- is independent of the value of the inter-leaflet friction coefficient.

As seen in Fig. 6, the λ -dependence of the diffusion coefficient for the supported case is well captured by that obtained in the limit of $\eta_f^+ \rightarrow 0$. Both of these cases have a large asymmetry between D^+ and D^- as the friction between the leaflets changes. This implies that contribution to friction from the fluid above the bilayer is small, and the friction from the lower fluid is dominant. D^- has a very low friction dependence and does not change much by changing λ .

The λ -dependence can be rationalized by taking the limits. In the limit of $\lambda \rightarrow \infty$,

Eq. (22a) becomes,

$$D_{sup}^{\alpha} = \frac{k_B T}{2\pi\eta\rho^2} \int_0^{\infty} d\kappa \frac{[J_1(\kappa\rho)]^2}{\kappa} \frac{1}{\kappa^2 + 1/(2h)} \quad (26)$$

$$= \frac{k_B T H}{2\pi\eta_f R^2} \left(\frac{1}{2} - I_1 \left(R \sqrt{\frac{\nu}{2H}} \right) K_1 \left(R \sqrt{\frac{\nu}{2H}} \right) \right). \quad (27)$$

Figure 6 shows that for very large values of λ , D^+ and D^- converge to the same value for both the cases. This is because the leaflets are moving together and losing their bilayer nature due to the high inter-leaflet friction. Whereas in the limit of $\lambda \rightarrow 0$, D_{sup}^+ in Eq. (22a) shows a divergence, and D_{sup}^- in Eq. (22a) reduces to the same expression as Eq. (27) with $\nu/2$ replaced by ν . This replacement implies that the monolayer thickness should be used instead of the bilayer thickness to obtain the membrane viscosity in the absence of the inter-leaflet friction. Note that the 2D-membrane viscosity is its 3-D viscosity multiplied by the membrane thickness. The slight change of D_{sup}^- in Fig. 6 is the result of the change in the hydrodynamic screening length from $2/\nu$ to $1/\nu$.

The diffusion coefficient as a function of ρ for a supported bilayer is shown in Fig. 7. We note that the difference between D^+ and D^- increases for both cases with increasing ρ as shown in Fig. 7. This implies that smaller sized domains have lower asymmetry between the upper and the lower leaflets, and it increases with increasing the size of the domain.

V. CORRELATED DYNAMICS BETWEEN TWO LEAFLETS

So far, we have studied the diffusion of a liquid domain in either side of the leaflet of bilayer. According to the strength of the inter-leaflet coupling, the diffusion in a leaflet influences the diffusion in another leaflet. In this section, we study the correlated diffusion of two point particles in different leaflets.

We define the x -axis using the line connecting the initial positions of two particles. By introducing the mobility tensor [24, 40]

$$G_{ij}^{\alpha\beta}(\mathbf{k}) = M^{\alpha\beta}(k) \left(\delta_{ij} - \frac{k_i k_j}{k^2} \right), \quad (28)$$

where $M^{\alpha\beta}(k)$ is given in Eq. (A2), we can calculate the correlation between displacements, $\left\langle \Delta r_i^{(1)} \Delta r_j^{(2)} \right\rangle_r^{\alpha\beta} = 2k_B T t G_{ij}^{\alpha\beta}(r)$, by the inverse Fourier transformation.

We consider the longitudinal and transverse coupling of displacements for two particles. The longitudinal coupling diffusion coefficient is defined by $D_L^{\alpha\beta}(r) \equiv \left\langle \Delta r_x^{(1)} \Delta r_x^{(2)} \right\rangle_r^{\alpha\beta} / (2t)$

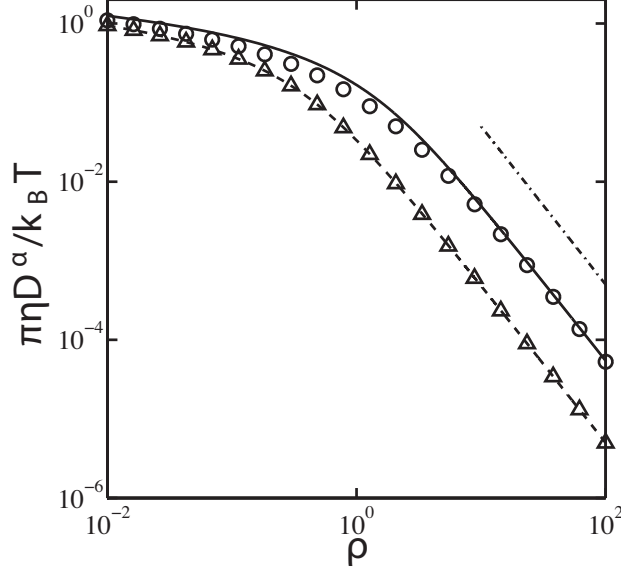


FIG. 7: $\pi\eta D^\alpha/k_B T$ as a function of ρ is shown for $h = 0.1$ and $\lambda = 1$ for the supported case and in the limit of $\eta_f^+ \rightarrow 0$. D^+ and D^- are shown by circular and triangular markers for the supported case, whereas they are shown by the solid and dashed lines in the limit of $\eta_f^+ \rightarrow 0$, respectively. $1/\rho^2$ is shown by a dash-dot line.

and is expressed as,

$$D_L^{\alpha\beta}(r) = k_B T \int_0^\infty \frac{dk}{2\pi} \frac{J_1(kr)}{r} M^{\alpha\beta}(k). \quad (29)$$

On the other hand, the transverse coupling diffusion coefficient is defined by $D_T^{\alpha\beta}(r) \equiv \langle \Delta r_y^{(1)} \Delta r_y^{(2)} \rangle_r^{\alpha\beta} / (2t)$ and is expressed as,

$$D_T^{\alpha\beta}(r) = k_B T \int_0^\infty \frac{dk}{2\pi} \frac{\partial J_1(kr)}{\partial r} M^{\alpha\beta}(k), \quad (30)$$

where $\partial J_1(z)/\partial z = J_0(z) - J_1(z)/z$ should be noted [41]. Using appropriate function for $M^{\alpha\beta}(k)$, the above expressions can be evaluated for all the cases discussed in the previous sections.

As a relevant example, we calculate the coupling displacements for the supported case mentioned in section IV. Using the appropriate mobility tensor, we obtain the longitudinal diffusion coefficient by using Mathematica as [42]

$$D_L^{\alpha\beta}(r) = \frac{k_B T}{4\pi\eta\rho} \sum_{i=1}^4 \frac{h^{\alpha\beta}(\omega_i)}{f'(\omega_i)} \left[\frac{-2}{\omega_i\rho} + \pi \{Y_1(-\omega_i\rho) + \mathbf{H}_{-1}(-\omega_i\rho)\} \right], \quad (31)$$

where $h^{\alpha\beta}(x) = g^\alpha(x)\delta_{\alpha\beta} + \lambda(1 - \delta_{\alpha\beta})$, and ω_i , $g^\alpha(x)$ and $f(x)$ were defined in Eq. (18). $Y_1(z)$ is the Bessel function of the second kind of order 1, and $\mathbf{H}_{-1}(z)$ is the Struve H-function of

order -1 [41]. Here, ρ denotes the distance between two particles normalized by ν , $\rho = \nu r$. The transverse coupling diffusion coefficient is calculated from Eq. (30) by changing the order of integration and differentiation [42]

$$D_T^{\alpha\beta}(r) = \frac{k_B T}{8\pi\eta} \sum_{i=1}^4 \frac{\omega_i h^{\alpha\beta}(\omega_i)}{f'(\omega_i)} \left[\frac{2(2 + \omega_i \rho)}{(\omega_i \rho)^2} - \pi \{Y_0(-\omega_i \rho) - Y_2(-\omega_i \rho) + \mathbf{H}_{-2}(-\omega_i \rho) - \mathbf{H}_0(-\omega_i \rho)\} \right]. \quad (32)$$

Equations (31)-(32) are obtained for point particles and valid without any restrictions on the separation distance. We study the above equations by taking the limits for ρ . Equations (31) and (32) become

$$D_{L,T}^{\alpha\beta}(r) \approx \frac{k_B T}{4\pi\eta} \sum_{i=1}^4 \frac{\omega_i h^{\alpha\beta}(\omega_i)}{f'(\omega_i)} \left[\ln \left(\frac{-2}{\omega_i \rho} \right) - \gamma \pm \frac{1}{2} \right], \quad (33)$$

in the limit of $\omega_i \rho \ll 1$, and

$$D_{L,T}^{\alpha\beta}(r) \approx \frac{k_B T}{2\pi\eta\rho^2} \sum_{i=1}^4 \left(\frac{\mp h^{\alpha\beta}(\omega_i)}{\omega_i f'(\omega_i)} \right), \quad (34)$$

in the limit of $\omega_i \rho \gg 1$. The upper and lower sign corresponds to the longitudinal and transverse component, respectively.

The correlated diffusion coefficients as a function of the frictional coupling are shown in Fig. 8. From Fig. 8 (a), we note that the longitudinal correlated diffusion exhibits a similar behavior as the diffusion coefficient if $\alpha = \beta$. As the value of the frictional coupling increases, the correlation decreases when the particles are in the same leaflet, whereas it increases when the particles are in the different leaflets. It is seen that the correlated diffusion between two particles in the different leaflets is small when $\lambda \leq 1$. However, as the value of the frictional coupling increases, the correlated diffusion coefficient in the different leaflets tends to converge to the smaller value of the correlated diffusion in the same leaflet.

As shown in Fig. 8 (b), the transverse components show some interesting features. For particles in the same leaflet, the correlation reduces from a positive value to a negative value for particles in the upper leaflet on increasing inter-membrane friction, while the correlation remains negative and approaches the value of the upper leaflet when particles are in the lower leaflet.

The correlated diffusion coefficients as a function of the separation between two inclusions are shown in Fig. 9. The longitudinal correlated diffusion exhibits a similar behavior as the

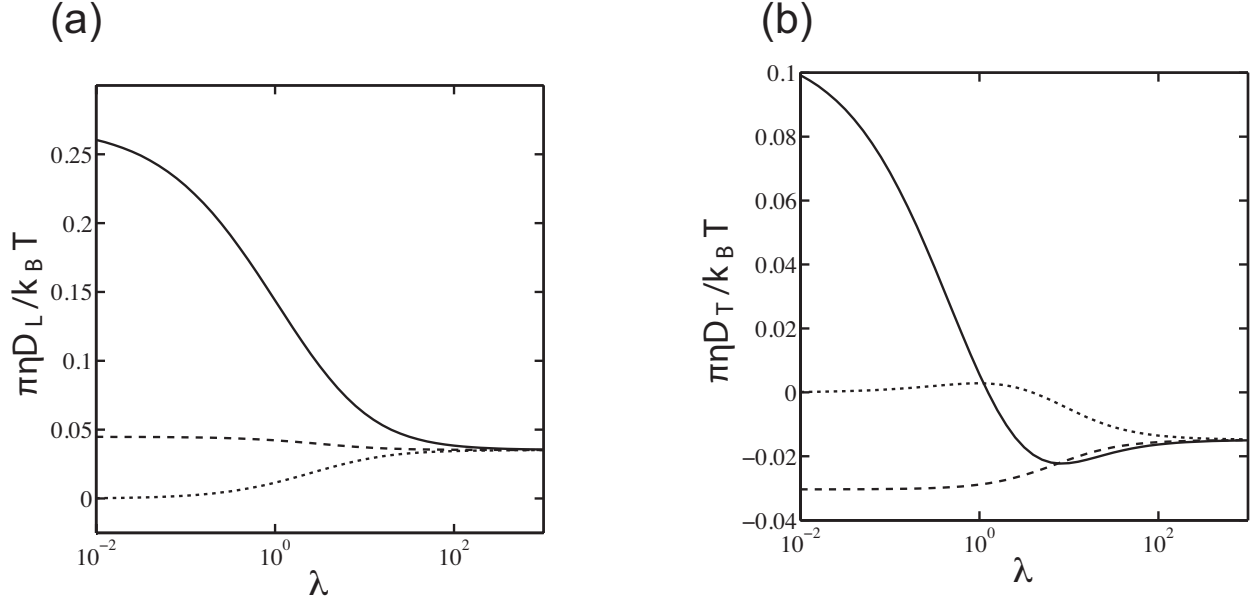


FIG. 8: The (a) longitudinal and (b) transverse correlation as a function of λ calculated from Eq. (31) and Eq. (32), respectively. The solid line indicates the case that both particles are embedded in the upper leaflet, whereas the dashed line indicates the case that both particles are embedded in the lower leaflet. The dotted line indicates that two particles are embedded in different leaflets. Parameters used are $h = 0.1$, $\rho = 1$.

diffusion coefficient. The transverse component decreases to a negative value and turns to increase as the separation increases if $\alpha = \alpha'$. In the description of the bilayer as a uniform 2D fluid, a similar non-monotonic dependence of the coupling diffusion coefficients on the separation between the inclusions has been reported [3]. The correlated diffusion coefficient in different leaflets monotonically decreases to zero by increasing the separation.

VI. SUMMARY AND DISCUSSION

We have investigated the effect of inter-leaflet friction on the domain diffusion in a leaflet of a bilayer. We considered both symmetric and asymmetric environments of solvents. For both cases, we have shown that the effect of the inter-leaflet friction on the leaflet diffusion is important if λ is smaller than $\lambda_2^* = 1/(2h)$; the value is taken from the inflection point of diffusion coefficient as a function of the inter-leaflet friction for large domains (see Appendix C for details). For small domains, the inflection point can be characterized by

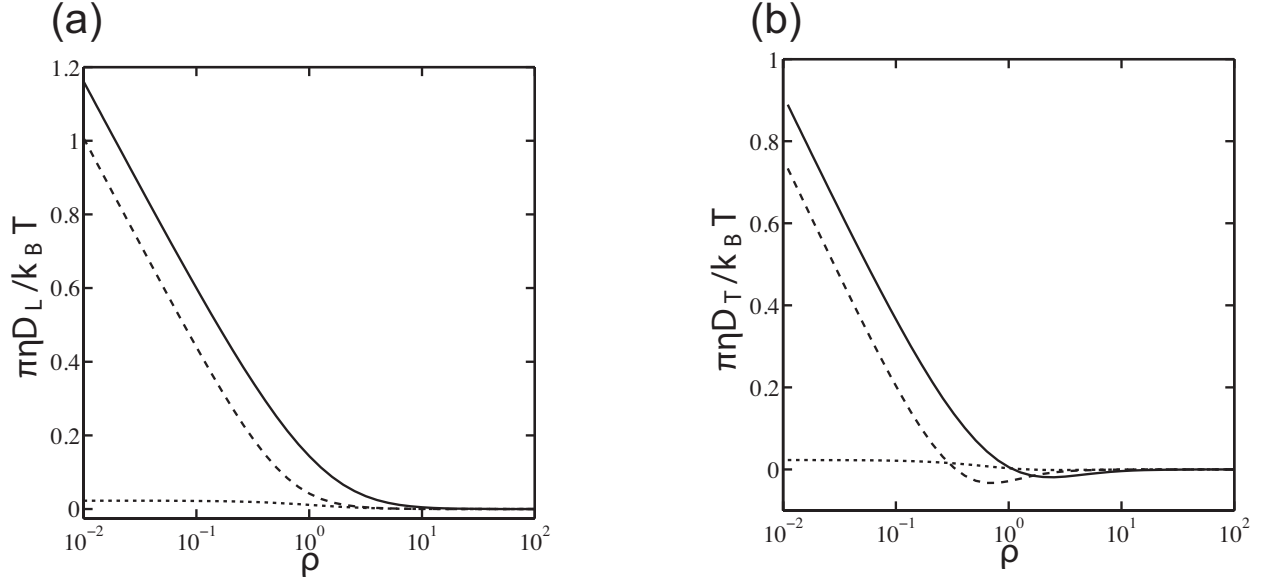


FIG. 9: The (a) longitudinal and (b) transverse correlation as a function of ρ calculated from Eq. (31) and Eq. (32), respectively. The solid line indicates the case that both particles are embedded in the upper leaflet, whereas the dashed line indicates that both particles are embedded in the lower leaflet. The dotted line indicates that two particles are embedded in different leaflets. Parameters used are $h = 0.1$, $\lambda = 1$.

$\lambda_1^* = (1/\rho - \cot(h/\rho))/(2\rho)$. The critical domain size can be obtained from $\lambda_1^* = \lambda_2^*$. We have also studied the size dependence of the leaflet-diffusion coefficient.

According to recent experiments, the value of inter-leaflet friction is estimated to be $\Lambda \sim 10^8 - 10^9$ Pa·s/m [26, 29, 33, 44]. The relation, $\lambda_2^* = 1/(2h)$, can be rewritten as $\Lambda^* = \eta_f/(2H)$. By substituting the typical values, $\eta_f \sim 1 \times 10^{-3}$ Pa·s and $H \sim 1$ nm, we find $\Lambda^* \approx 5 \times 10^5$ Pa·s/m. However, if solvents are confined in molecular scales, the solvent viscosity is reported to be significantly increased, $\eta_f \sim 0.1$ Pa·s [24, 30]. In the extremely confined situation, Λ^* can be increased to 5×10^7 Pa·s/m. Experimental values of $\Lambda \sim 10^8 - 10^9$ Pa·s/m is not much different from the value of Λ^* for the extremely confined case. The value of λ_1^* relevant to the small size of diffusing objects can be order of magnitude larger than that of λ_2^* . For small domains, by using λ_1^* we estimate that Λ^* can be 10^9 Pa·s/m for the extremely confined case and 10^7 Pa·s/m without molecular scale confinements.

According to simulations, the value of inter-leaflet friction is reported to be $\Lambda \sim 2.4 \times 10^6$

Pa·s/m [34, 35]. There, the leaflet diffusion at small sizes can be affected by the inter-leaflet friction. Indeed, the lateral diffusion of the lower leaflet was shown to be slower than that of the upper leaflet by the attractive interaction of the support within a coarse-grained molecular simulation [36].

In this paper, we have studied asymmetry in leaflet diffusion coefficients induced by the asymmetry in environments. By anchoring lipopolymer, the fluidity of a leaflet composing a bilayer can be obstructed and the fluidity of leaflets can be asymmetric [45, 46]. When the fluidity of leaflets is asymmetric, the inter-leaflet friction should be in principle taken into account. Although the model studied in this paper is simpler than the situation of lipopolymer-grafted bilayers, our study could be useful to understand the effect of the asymmetry in the fluidity between two leaflets on the leaflet diffusion.

Finally, we discuss the diffusion of a circular liquid domain in an isolated membrane without any solvent to study the actual contribution of the momentum dissipation by the inter-leaflet friction. In the absence of the coupling to 3D solvent, the SD length given by the ratio between the 2D membrane viscosity and the 3D solvent viscosity diverges. This divergence reflects the so-called Stokes paradox; the diffusion coefficient cannot be obtained by solving hydrodynamic equation in the limit of low-Reynolds number in pure 2D fluid since the influence of translational motion of a circular body extends to large distances due to lack of enough momentum dissipation in 2D. Although the coupling between solvents and the bilayer is absent, the momentum can be dissipated through the inter-leaflet friction. In order to see whether the Stokes paradox can be resolved by inter-leaflet friction alone, we set $\eta_f^\pm = 0$ in Eq. (3) resulting,

$$D = \frac{k_B T}{\pi R^2} \int_0^\infty dk \frac{[J_1(kR)]^2}{k} \left[\frac{\eta_- k^2 + b}{k^2 (\eta^+ \eta^- k^2 + \Lambda \eta^+ \eta^-)} \right]. \quad (35)$$

The above expression can be rewritten as

$$D = \frac{k_B T}{\pi R^2} \frac{1}{\eta^+ + \eta^-} \left\{ \int_0^\infty dk \frac{[J_1(kR)]^2}{k^3} + \frac{\eta^-}{\eta^+} \int_0^\infty dk \frac{[J_1(kR)]^2}{k} \left[\frac{1}{k^2 + \Lambda(\eta^+ + \eta^-)/(\eta^+ \eta^-)} \right] \right\}. \quad (36)$$

In Eq. (36), we note that the first term diverges at $k = 0$, because $J_1(z) \approx z$ when $z \ll 1$ and $J_1(kR)^2/k^3 \approx 1/k$ in this limit. This shows that frictional coupling of leaflets is not enough to provide for a finite diffusion coefficient, and contribution from solvents is essential. We get an interesting result if we allow $\eta^- \rightarrow \infty$, which implies that the lower leaflet of the

membrane behaves as a solid. In this limit, we obtain

$$D = \frac{k_B T}{\pi R^2} \int_0^\infty dk \frac{[J_1(kR)]^2}{k} \left[\frac{1}{\eta^+ k^2 + \Lambda} \right]. \quad (37)$$

Equation (37) does give a finite result for the diffusion coefficient, which can be explained by the lower leaflet providing required friction for diffusion, instead of the solvent.

In the above, we show that the frictional coupling between two leaflets alone is not enough to resolve the Stokes paradox. Only in the case that one of the leaflet of the membrane is immobile, a finite diffusion coefficient can be obtained without solvents. The particular model was already applied to study the inter-leaflet friction from the diffusion in a leaflet coupled to an immobile leaflet [47], and the diffusion in a polymer-supported monolayer where the polymer plays the roll of an immobile leaflet [48]. However, if both leaflets are viscous, the model should include the coupling to solvents to have finite diffusion coefficients.

Acknowledgments

KS and SK are supported by Grant-in-Aid for Scientific Research (grant No. 24540439) from the MEXT of Japan. This research was conducted under Agreement for Collaboration between IIT Bombay and Nanosystem Research Institute, AIST. SK would like to acknowledge support from the Grant-in-Aid for Scientific Research on Innovative Areas "Fluctuation & Structure" (No. 25103010) from the MEXT of Japan, and the JSPS Core-to-Core Program "International research network for nonequilibrium dynamics of soft matter".

Appendix A: Velocity field

Denoting the total force on the circular domain in the steady state by \mathbf{F}^\pm , the velocity field is expressed as [49]

$$\mathbf{v}^\alpha(\mathbf{r}) = - \left[\int_0^\infty dk M^{\alpha\alpha}(k) \frac{J_1(kR)J_1(kr)}{\pi k R r} \hat{\mathbf{e}}_x + \int_0^\infty dk M^{\alpha\alpha}(k) \frac{J_1(kR)J_2(kr) \sin(\theta)}{\pi R} \hat{\mathbf{e}}_\theta \right] F^\alpha, \quad (\text{A1})$$

where $\hat{\mathbf{e}}_x$ is the unit vector in the direction of the x -axis, $\hat{\mathbf{e}}_\theta$ is the unit vector tangential to the circle pointed in the direction of rotation, indices α, β denote the leaflets. In the above equation, $M^{\alpha\beta}(k)$ represents a component of a mobility tensor in Fourier space and is given

by [24]

$$M^{\alpha\beta}(k) = \frac{[\eta^{(-\alpha)}k^2 + \eta_f^{(-\alpha)}k \coth(kH^{(-\alpha)})]\delta_{\alpha\beta} + \Lambda}{\prod_{\alpha}(\eta^{(\alpha)}k^2 + \eta_f^{(\alpha)}k \coth(kH^{(\alpha)}) + \Lambda) - \Lambda^2}, \quad (\text{A2})$$

where $(-\alpha)$ represents the leaflet opposite to α .

By noticing that the velocity at $(R, 0)$ is equal to \mathbf{U} , the friction coefficient, ζ , is obtained from the linear relation, $\mathbf{U} = -(1/\zeta)\mathbf{F}$. Using the Einstein relation $D = k_B T/\zeta$ [50], we obtain the diffusion coefficient as in Eq. (3).

The velocity fields can be drawn by using Eq. (A1). As an example, we draw the velocity fields for the supported case of Sec. IV. The velocity field in the lower leaflet is shown when a liquid domain is located in the upper (lower) leaflet in Fig. 10. By comparing the velocity fields, we could see that a part of the velocity field in the lower leaflet flows opposite to the flow velocity of the liquid domain compared to that in the upper leaflet.

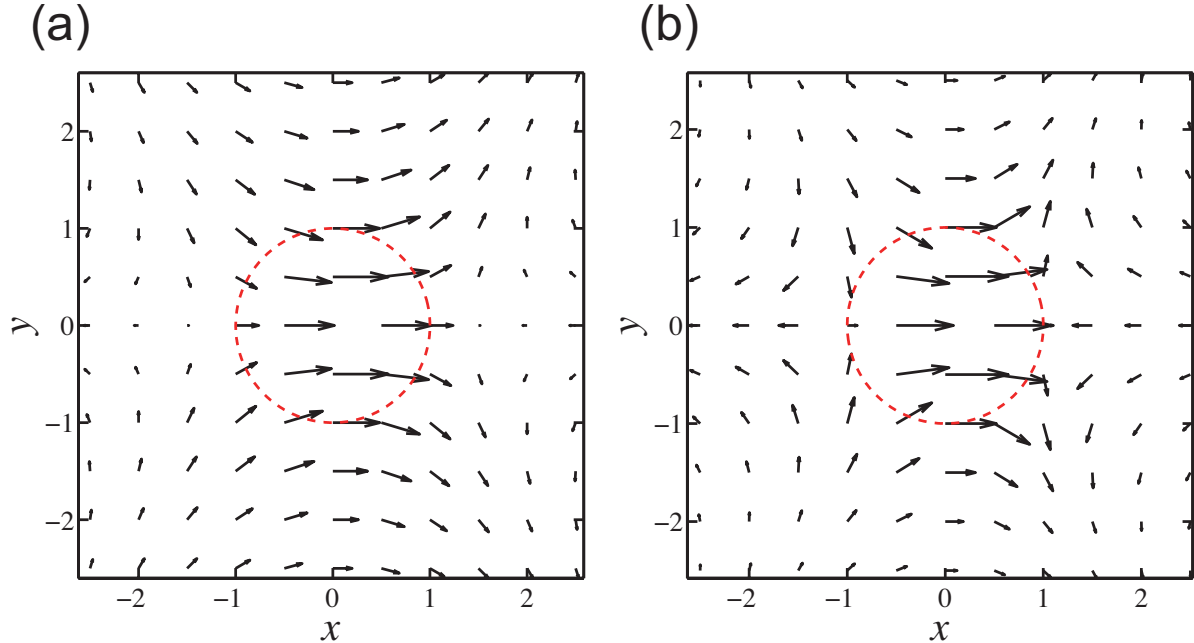


FIG. 10: Velocity field for the supported case calculated from Eq. (18) when the domain is in the (a) upper and (b) lower leaflets. The center of the domain moves with the velocity \mathbf{U} in the positive direction of the x -axis. Parameters used are $h = 0.1$, $\rho = 1$, $\lambda = 1$.

Appendix B: Partial Fraction expansion to solve required integrals

We now derive the result in Eq. (15) from Eqs. (5) and (6) using the method of partial fractions. A general relation used to obtain partial fraction expansion for $g(x)/f(x)$ is [51]

$$\frac{g(x)}{f(x)} = \sum_{\text{all roots}} \frac{g(x_i)}{f'(x_i)} \frac{1}{(x - x_i)}, \quad (\text{B1})$$

where x_i are the roots of the denominator, $f(x)$, and the sum is carried out over all roots. We find the partial fraction expansion for the $D_1(\lambda)$ term in Eq. (5). The other term can be obtained by putting $\lambda = 0$ and following the same procedure. The fraction under consideration is $1/(\kappa^2 + \kappa \coth(\kappa h) + 2\lambda)$. Equating the denominator to zero, we obtain,

$$\kappa_s^2 + \kappa_s \coth(\kappa_s h) + 2\lambda = 0, \quad (\text{B2})$$

where ‘ s ’ is the index of the root. It is convenient to introduce a transformation $\kappa_s = i\omega_s$ when an infinite number of roots exists. This gives,

$$\omega_s^2 = \omega_s \cot(\omega_s h) + 2\lambda. \quad (\text{B3})$$

We substitute $\cot(\omega_s h) = (\omega_s^2 - 2\lambda)/\omega_s$ in Eq. (B1) to obtain,

$$\frac{1}{\kappa^2 + \kappa \coth(\kappa h) + 2\lambda} = \sum_{s=-\infty}^{\infty} \left(\frac{1}{h\omega_s^4 + (1 + h - 4\lambda h)\omega_s^2 + 2\lambda + 4h\lambda^2} \right) \frac{\omega_s/i}{\kappa - i\omega_s}, \quad (\text{B4})$$

where we can assume $\omega_{-s} = -\omega_s$ without loss of generality. Since the expression within the parenthesis is even, we obtain

$$\frac{1}{\kappa^2 + \kappa \coth(\kappa h) + 2\lambda} = \sum_{s=1}^{\infty} \left(\frac{2\omega_s^2}{h\omega_s^4 + (1 + h - 4\lambda h)\omega_s^2 + 2\lambda + 4h\lambda^2} \right) \frac{1}{\kappa^2 + \omega_s^2}. \quad (\text{B5})$$

If the first term in the expansion dominates, Eq. (6) becomes

$$D_1(\lambda) = \frac{k_B T}{\pi \eta \rho^2} \frac{2}{h\omega_1^4 + (1 + h - 4\lambda h)\omega_1^2 + 2\lambda + 4h\lambda^2} \left[\frac{1}{2} - I_1(\omega_1 \rho) K_1(\omega_1 \rho) \right]. \quad (\text{B6})$$

Appendix C: Inflection point of the diffusion coefficient as a function of λ

The inflection region for the diffusion coefficient as a function of λ is very different when $\rho \ll 1$ in Fig. 3. The inflection originates from the variation of the Bessel functions. When $\omega_1 \rho \ll 1$, the term including Bessel functions can be approximated by a logarithmic function

of the variable by using the expansion, $I_1(z)K_1(z)/z^2 \sim (1/4) \ln z$ for $z \leq 1$. The logarithmic dependence is weak and the condition, $\omega_1\rho \gg 1$, should be satisfied to obtain sharp variable dependence from the Bessel functions. By substituting $\omega_1\rho \sim 1$ into the characteristic equation, Eq. (17), we obtain $\lambda_1^* = [1/\rho - \cot(h/\rho)]/(2\rho)$. At the inflection point, the term including Bessel functions should depend sharply on the variables and the variable itself should depend sharply on the value of λ .

We now discuss the λ -dependence of the variable $\omega_1\rho$. In the limit of $h \rightarrow 0$, we have $\cot(h/\rho) \sim \rho/h$ and obtain, $\omega_1\rho \sim \left(\rho/\sqrt{h}\right) \sqrt{1+2\lambda h}$. Therefore, the variable, $\omega_1\rho$, depends largely on λ if λ value exceeds $\lambda_2^* = 1/(2h)$. By comparison, we note that λ_2^* can be used even when h is as large as 10. In summary, the larger of λ_1^* or λ_2^* characterizes the inflection point. When ρ is small, the inflection point is characterized by λ_1^* . By increasing ρ , λ_1^* decreases and the inflection point is characterized by λ_2^* . The switching between λ_1^* and λ_2^* takes place at ρ satisfying $\lambda_1^* = \lambda_2^*$. As seen in Fig. 3, if the inflection point is characterized by λ_1^* , the inflection point can become order of magnitude larger than λ_2^* by decreasing ρ .

The value characterizing the inflection point, λ_2^* , can be obtained by equating the inter-leaflet sliding length, $\sqrt{\eta/b}$, with the ES hydrodynamic screening length, \sqrt{h}/ν . The velocity field in the membrane perturbed by a diffusing particle is 2D-like within the ES length and becomes 3D-like if the distance from the diffusing particle exceeds the ES length. If the inter-leaflet sliding length is smaller than the ES length, 2D-like feature of the velocity field is not affected by inter-leaflet sliding. On the other hand, if the inter-leaflet sliding length is larger than the ES length, 2D-like feature of the velocity field is largely influenced by the inter-leaflet sliding and the diffusion coefficient is increased by the sliding effect.

-
- [1] P. G. Saffman and M. Delbrück, Proc. Natl. Acad. Sci. USA **72**, 3111 (1975).
 - [2] P. G. Saffman, J. Fluid Mech. **73**, 593 (1976).
 - [3] N. Oppenheimer and H. Diamant, Phys. Rev. E **82** 041912 (2010).
 - [4] B. D. Hughes, B. A. Pailthorpe, and L. R. White, J. Fluid Mech. **110** 349 (1981).
 - [5] Y. Gambin, R. Lopez-Esparza, M. Reffay, E. Sierrecki, N.S. Gov, M. Genest, R.S. Hodges, W. Urbach, Proc. Natl. Acad. Sci. U.S.A. **103**, 2098 (2006).
 - [6] P. Cicuta, S. L. Keller, S. L. Veatch, J. Phys. Chem. B. **111** 3328 (2007).

- [7] E. P. Petrov and P. Schwille, *Biophys J.* **94** L41 (2008).
- [8] S. Ramadurai, A. Holt, V. Krasnikov, G. van den Bogaart, J. A. Killian, and B. Poolman, *J. Am. Chem. Soc.* **131** 12650 (2009).
- [9] E. Evans and E. Sackmann, *J. Fluid. Mech.* **194** 553 (1988).
- [10] H. A. Stone and A. Ajdari, *J. Fluid Mech.* **369** 151 (1998).
- [11] F. Harb, J. Sarkis, N. Ferte, and B. Tinland, *Eur. Phys. J. E* **35** 118 (2012).
- [12] K. Simons and E. Ikonen, *Nature* **387** 569 (1997).
- [13] D. Lingwood and K. Simons, *Science* **327** (2010) 46.
- [14] D. W. Allender and M. Schick, *Biophys. J.* **91** 2928 (2006).
- [15] M. D. Collins and S. L. Keller, *Proc. Natl. Acad. Sci. USA* **105** 124 (2008).
- [16] R. De Koker, Ph.D. thesis, Stanford University, 1996.
- [17] S. Ramachandran, S. Komura, M. Imai, and K. Seki, *Eur. Phys. J. E* **31** 303 (2010).
- [18] K. Seki, S. Ramachandran, and S. Komura, *Phys. Rev. E* **84** 021905 (2011).
- [19] Y. Fujitani, *J. Phys. Soc. Jpn.* **81** 084601 (2012).
- [20] Y. Fujitani, *J. Phys. Soc. Jpn.* **82** 084403 (2013).
- [21] U. Seifert and S. Langer, *Europhys. Lett.* **23** 71 (1993).
- [22] H. A. Stone and H. M. McConnell, *Proc. R. Soc. London A* **448** 97 (1995).
- [23] A. J. Levine and F. C. MacKintosh, *Phys. Rev. E* **66** 061606 (2002).
- [24] B. A. Camley and F. L. H. Brown, *Soft Matter* **9** 4767 (2013).
- [25] T. Han, and M. Haataja, *Soft Matter*, **9**, 2120 (2013).
- [26] E. Evans and A. Yeung, *Chem. Phys. Lipids* **73** 39 (1994).
- [27] R. M. Raphael and R. E. Waugh, *Biophys. J.* **71** 1374 (1996).
- [28] T. Pott and P. Méléard, *Europhys. Lett.* **59** 87 (2002).
- [29] A. F. Bitbol, J. B. Fournier, M. I. Angelova and N. Puff, *J. Phys.: Condens. Matter*, **23** 284102 (2011).
- [30] L. Zhang and S. Granick, *J. Chem. Phys.* **123** 211104 (2005).
- [31] C. Scomparin, S. Lecuyer, M. Ferreira, T. Charitat, and B. Tinland, *Eur. Phys. J. E* **28** 211 (2009).
- [32] M. Hetzer, S. Heinz, S. Grage, and T.M. Bayerl, *Langmuir* **14** 982 (1998).
- [33] R. Macháň and M. Hof, *Biochimica et Biophysica Acta* **1798** 1377 (2010).
- [34] S. A. Shkulipa, W. K. den Otter, and W. J. Briels, *Phys. Rev. Lett.* **96** 178302 (2006).

- [35] W. K. den Otter and S. A. Shkulipa, *Biophys. J.* **93** 423 (2007).
- [36] C. Xing and R. Faller, *J. Phys. Chem. B* **112** 7086 (2008).
- [37] K. Inaura and Y. Fujitani, *J. Phys. Soc. Jpn.* **77** 114603 (2008).
- [38] D. K. Lubensky and R. E. Goldstein, *Phys. Fluids* **8** 843 (1996).
- [39] Th. M. Fischer, *J. Fluid Mech.* **498** 123 (2004).
- [40] S. Ramachandran, S. Komura, K. Seki and G. Gompper, *Eur. Phys. J. E* **34** 46 (2011).
- [41] Abramowitz M and Stegun I A, *Handbook of Mathematical Functions* (Dover, New York,1972).
- [42] Wolfram Research Inc., *MATHEMATICA 9* (Wolfram Research, Champaign, 1988).
- [43] In Eq. (39) of Ref. [18], the term proportional to $1/R^4$ should be eliminated. This is due to an error in *MATHEMATICA 7*. The other parts including Eqs. (40)-(44) are not affected by the correction.
- [44] J. B. Fournier, N. Khalifat, N. Puff and M. I. Angelova, *Phys. Rev. Lett.* **102** 018102 (2009).
- [45] M. Tanaka and E. Sackmann, *Nature* **437** 656 (2005).
- [46] H.-Y. Zhang and R. J. Hill, *J. R. Soc. Interface* **8** 127 (2011).
- [47] R. Merkel, E. Sackmann, and E. Evans, *J. Phys. France* **50** 1535 (1989).
- [48] M. Tanaka, J. Hermann, I. Haase, M. Fischer, and S. G. Boxer, *Langmuir* **23** 5638 (2007).
- [49] This result is the correction of a similar result from a previous publication [18]. The velocity at $(R, 0)$ was correct and the other parts are not affected by the correction in [18].
- [50] R. Kubo, M. Toda, and N. Hashitsume, *"Statistical Physics II: Nonequilibrium Statistical Mechanics"* (Springer-Verlag,Berlin,1992).
- [51] G. B. Arfken and H. J. Weber, *Mathematical Methods for Physicists*, 5th ed., (Academic, San Diego, California, 2001).